

# Wireless Power and Data Transfer via a Common Inductive Link Using Frequency Division Multiplexing

Jiande Wu, *Member, IEEE*, Chongwen Zhao, *Student Member, IEEE*,  
Zhengyu Lin, *Senior Member, IEEE*, Jin Du, *Student Member, IEEE*,  
Yihua Hu, *Member, IEEE*, and Xiangning He, *Fellow, IEEE*

**Abstract**—For wireless power transfer (WPT) systems, communication between the primary side and the pickup side is a challenge because of the large air gap and magnetic interferences. A novel method, which integrates bidirectional data communication into a high-power WPT system, is proposed in this paper. The power and data transfer share the same inductive link between coreless coils. Power/data frequency division multiplexing technique is applied, and the power and data are transmitted by employing different frequency carriers and controlled independently. The circuit model of the multiband system is provided to analyze the transmission gain of the communication channel, as well as the power delivery performance. The crosstalk interference between two carriers is discussed. In addition, the signal-to-noise ratios of the channels are also estimated, which gives a guideline for the design of mod/demod circuits. Finally, a 500-W WPT prototype has been built to demonstrate the effectiveness of the proposed WPT system.

**Index Terms**—Frequency division multiplexing, multiband system, near-field magnetic communication, wireless power and data transfer.

## I. INTRODUCTION

WITH the development of electronics, the wireless power transfer (WPT) technology has been widely adapted for advantages of convenience and safety. Since the 1960s, the WPT technique has been applied in biomedical fields, which made great progress for human health care [1], [2]. In the field of consumer electronics, the wireless charger is becoming popular, and several WPT standards have been set up to increase the interoperability of different chargers [3]–[5]. For high-power application such as electrical vehicles chargers and grids

interface [6]–[11], the WPT technique enhances the devices safety and decreases the connectivity complexity.

For most applications, reliable communication between the primary side and the pickup side plays an essential role in a well-designed WPT system. For instance, the functions such as output voltage feedback control, load detection, status monitoring, autotuning, and multicontrollers synchronization are generally required in WPT systems [12]–[17], which can be implemented more easily if the communication between both sides is provided. Radio-frequency (RF) link is a common way employed in many WPT systems for wireless communication [12], [13], but it leads to higher costs and lower reliability with an increasing power rating of WPT system.

Several methods have been proposed to transfer power and data from the same inductive link. For example, in some low-power cases, the inherent inductive link for power transfer is exploited as an antenna for data transmission, where the data is directly modulated on the power carrier by frequency shifting keying (FSK) in forward data transmission, and the load-shift keying (LSK) technique is adopted to achieve backward data transmission [18]. However, the techniques that employ a single carrier for both power and data transfers have two major drawbacks. The first one is that the data rate is limited by the frequency of the carrier. For the systems using power-carrier frequency below 50 kHz, the data rate should not exceed several kb/s. The second drawback is that the FSK technique used for forward communication decreases the power transmission efficiency since the operation of system shifts from its optimal points; thus, FSK/LSK technique is not suitable for the application of high-power WPT system.

Several methods of using multiple inductive links with multiple carriers have been proposed to increase the data rate and maintain the efficiency of power transfer [19]–[24]. In these methods, power and data are transferred via independent physical channels, where the power carrier is delivered through one inductive link and the data carrier is transmitted via another. However, multiple links will cause extra magnetic interferences between the two channels. The strong power carrier is regarded as a large noise for a small data signal, which decreases the signal-to-noise ratio (SNR) in communication channel. Multiple inductive links also lead to larger device size, which is undesirable for confined space applications.

The scheme with multiple carriers in a single inductive link is another candidate for WPT systems, in which two tuning points

Manuscript received May 24, 2014; revised March 2, 2015 and May 4, 2015; accepted June 13, 2015. Date of publication July 9, 2015; date of current version November 6, 2015. This work was supported by the National Natural Science Foundation of China under Grant 61174157 and Grant 51361130150.

J. Wu, J. Du, and X. He are with the College of Electrical Engineering, Zhejiang University, Hangzhou 310027, China (e-mail: eewjd@zju.edu.cn; eedujin@zju.edu.cn; hxn@zju.edu.cn).

C. Zhao is with The University of Tennessee, Knoxville, TN 37996 USA (e-mail: zcwpxp@yahoo.com.cn).

Z. Lin is with Electrical, Electronic and Power Engineering, Aston University, Birmingham, B4 7ET, U.K. (e-mail: z.lin@ieee.org).

Y. Hu is with the Department of Electronic and Electrical Engineering, University of Strathclyde, Glasgow, G1 1XW, U.K.

Color versions of one or more of the figures in this paper are available online at <http://ieeexplore.ieee.org>.

Digital Object Identifier 10.1109/TIE.2015.2453934

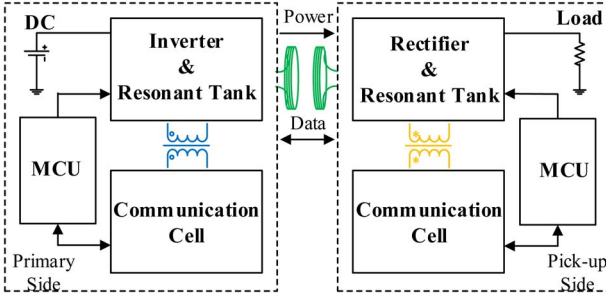


Fig. 1. Block diagram of wireless power and data transfer system.

in both sides facilitate the data transmission while eliminating extra coils. In [25]–[27], wireless power and data transmission is achieved between the primary and secondary side of a strong coupled inductor, whose air gap is less than 1 mm. In this method, a high-frequency data carrier is overlapped on the power carrier for communication during nonswitching period of the power inverter. This scheme is equally applicable for loosely coupled WPT systems [28], but detailed communication models and specific circuit designs are not discussed in previous papers.

In this paper, a novel system with multiple carriers in a single inductive link is proposed for wireless power and data transmission, and the detailed mathematical model of the proposed multiband system is presented and analyzed. This method is applicable for high-power WPT systems operating in several tens of kilohertz, and the data-carrier frequency is selected at least an order of magnitude higher than power frequency. There are several advantages compared with other methods. 1) The structure of the system is simple and no extra coil is needed. 2) The control of power converter and data communication is independent with each other. 3) The mutual inductance of the coils can be calculated on line by measuring the amplitude of the received data carrier, which can be utilized to estimate the distance of the two coils.

The crosstalk interference between power and data channel in the dual-tuning system that aims to achieve high power transmission efficiency and reliable bidirectional communication is discussed in detail. Moreover, a low-cost circuit design is provided to implement the proposed frequency division multiplexing technique. The effectiveness of the proposed WPT system is verified by experimental results from a 500-W WPT prototype.

## II. SYSTEM OVERVIEW

The block diagram of the proposed system is shown in Fig. 1. The system is divided into two parts, i.e., the primary side and the pickup side. The inductive link bridges the primary side and the pickup side, which is indispensable for WPT. A full-bridge inverter on the primary side delivers power to the load via the inductive coils, and a rectifier is employed on the pickup side to convert the inductive energy into dc output voltage.

The proposed communication cell, which is shown in Fig. 2, is adopted in both sides and magnetically coupled with power resonant tank by the ferrite-core coupled inductors. The com-

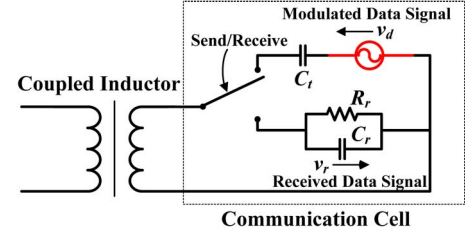


Fig. 2. Block diagram of communication cell structure.

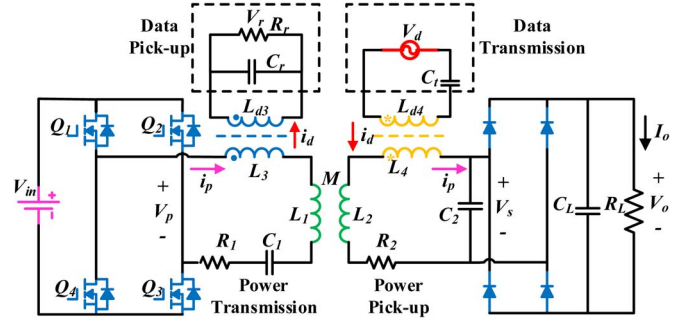


Fig. 3. Schematic circuit of the SP topology with backward communication.

munication cells have two operation modes: transmitter mode and receiver mode, which is controlled by an electronics switch. At transmitter mode, a signal amplifier is employed as a data source to transmit data. At receiver mode, an impedance matching network is connected to receive the data carrier from the other side, and the data is demodulated and read by an MCU. Thus, the system can work in two statuses, i.e., forward communication status and backward communication status. In forward communication status, the primary side is working on transmitter mode and the pickup side is working on receiver mode; in backward communication status, the primary side is working on receiver mode and the pickup side is working on transmitter mode.

For a WPT system, SS, SP, PP, and PS are basic structures that are classified according to the different  $LC$  branches (serial and parallel) in primary side and pickup side. The proposed communication cell can be inserted to a serial  $LC$  branch or a parallel  $LC$  branch; thus, the proposed method is applicable for SP, SS, PP, and PS topology WPT circuits. In this paper, the SP (primary series, secondary parallel compensation) topology is employed as an example of wireless power and data transfer system.

The schematic diagram of the proposed system is shown in Fig. 3 for backward communication and in Fig. 5(a) for forward communication.  $L_1$  and  $R_1$  are the inductor and resistor of the primary inductive coil, and  $C_1$  is the series compensation capacitor.  $L_2$  and  $R_2$  are the inductor and resistor of the pickup winding and  $C_2$  is the parallel compensation capacitor. The inductive coils are made of litz wire to reduce ac resistances.  $L_3$  and  $L_4$  are coupled inductors for data-carrier coupling. The frequency of power carrier is set at 22.4 kHz and the data carrier is set at 1.67 MHz. In the proposed method, the data-carrier frequency should be at least an order of magnitude higher than power frequency, that because: 1) only in this condition,

TABLE I  
CIRCUIT COMPONENTS OF THE PROPOSED SYSTEM

Components	Parameters
$L_1$ and $L_2$ (Inductive coil)	153 $\mu$ H
$C_1$ and $C_2$ (Compensation capacitor)	0.33 $\mu$ F
$L_m$ (Magnetizing inductor of coupled inductors)	3 $\mu$ H
$L_{lk}$ (Leakage inductor of coupled inductors)	0.8 $\mu$ H
$N$ (Turns ratio of coupled inductors)	4:4
$C_t$ and $C_r$ (Communication cell capacitor)	2.3nF
$R_r$ (Communication cell resistor)	10k $\Omega$

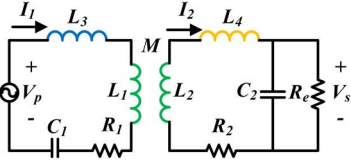


Fig. 4. SP compensation lumped-circuit model.

the voltage drop of power carrier on the communication cell is quite small; thus, the power transfer efficiency would not be significantly decreased by the communication cell; 2) the crosstalk interference of data communication from power transfer is suppressed to facilitate the design of demodulation circuit and guarantee the reliability of communication.

The specific parameters of the circuit are given in Table I.

### III. POWER DELIVERY ANALYSIS

Because extra communication components are added to the power resonant tank, it is necessary to evaluate the performance of power delivery and the cross effect introduced by the data transmission. In the following analysis, it is assumed that the data-carrier frequency is much higher than the power frequency, and the inductance of the signal coupled inductor is much lower than that of the inductive coil.

#### A. Coupled Inductor Impact

The circuit model of the SP topology is shown in Fig. 4.  $V_p$  is the inverter output voltage, which is simplified as a sinusoidal voltage source by neglecting higher order harmonics. The rectifier with load is simplified as an equivalent resistance  $R_e$ . In addition, at the power-frequency  $f_p$ , the impedances of the signal coupled inductor  $L_3$  and  $L_4$  are much smaller than the reflected impedances of  $C_t$  and  $C_r$ ; thus, the equivalent circuit of communication cells is simplified as an inductor.  $L_{3\sim4}$  are composed of the magnetizing inductor  $L_{m3\sim4}$  and leakage inductor  $L_{lk3\sim4}$ , which are involved in power resonance.

By analyzing the impacts of coupled inductors on power transfer operation in steady state and ignoring the data carrier, the circuit equations of Fig. 4 are

$$\begin{cases} V_p = \left( j\omega L_1 + j\omega L_3 + \frac{1}{j\omega C_1} + R_1 \right) I_1 - j\omega M I_2 \\ 0 = \left( j\omega L_2 + j\omega L_4 + \frac{1}{j\omega C_2 + 1/R_e} + R_2 \right) I_2 - j\omega M I_1. \end{cases} \quad (1)$$

When the switching frequency of the inverter is tuned to the circuit resonant frequency, the primary inductance ( $L_1 + L_3$ )

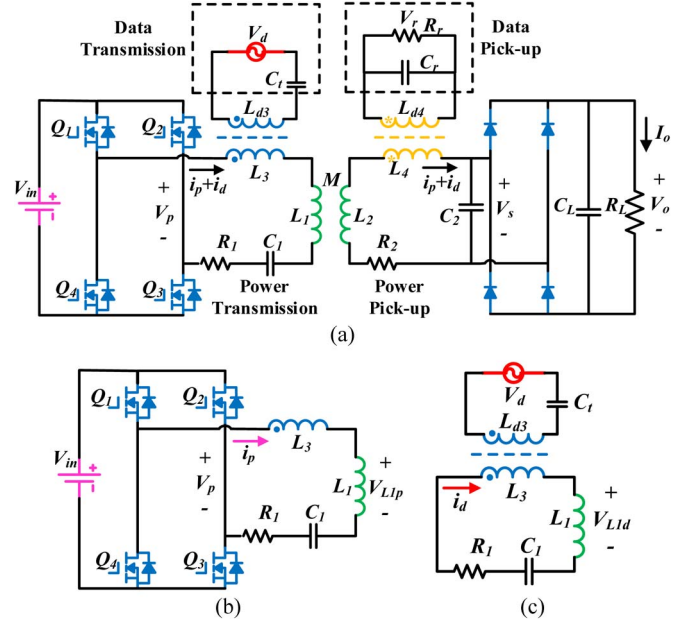


Fig. 5. (a) Schematic circuit with forward data transmission. (b) Power transfer equivalent circuit. (c) Data transmission equivalent circuit.

and the pickup side inductance ( $L_2 + L_4$ ) are compensated by  $C_1$  and  $C_2$ . The resonant angular frequency  $\omega_p$  of the proposed system is expressed as

$$\omega_p = \frac{1}{\sqrt{(L_1 + L_3)C_1}} = \frac{1}{\sqrt{(L_2 + L_4)C_2}}. \quad (2)$$

$L_3$  and  $L_4$  have a small number of turns and small ferrite-core volumes; thus, the copper loss and core loss of the coupled inductors have small influence on the power transmission efficiency and overall output power. If the losses on the coupled inductors are ignored, the power delivery performance of the proposed system is similar to the conventional circuits without communication, which is given in [7].

#### B. Operation Preconditions for Data Carrier

It is assumed that energy transfer is not influenced by data transmission in the proposed system. However, the data carrier could bring about interference to the inverter output and reduce the system efficiency. Here, the impact of the data carrier on the power transmission is discussed.

The schematic diagram of forward data transmission circuits is shown in Fig. 5(a). The primary side current is composed of two parts: power-carrier current  $i_p$  and data-carrier current  $i_d$ , which corresponding to the inductor current in Fig. 5(b) and (c).

Assuming the switches  $Q_{1-4}$  are ideal with no parasitic capacitor, the data carrier injected from the coupled inductor may change the current path, which causes voltage spikes in the inverter output. The voltage spikes would be induced if the two preconditions are satisfied. 1) During the dead time of the two legs, the current is approaching to zero, which means that the equivalent load of the inverter is almost resistive. 2) The current slew rate of data carrier is higher than that of the power current at the period of dead time.



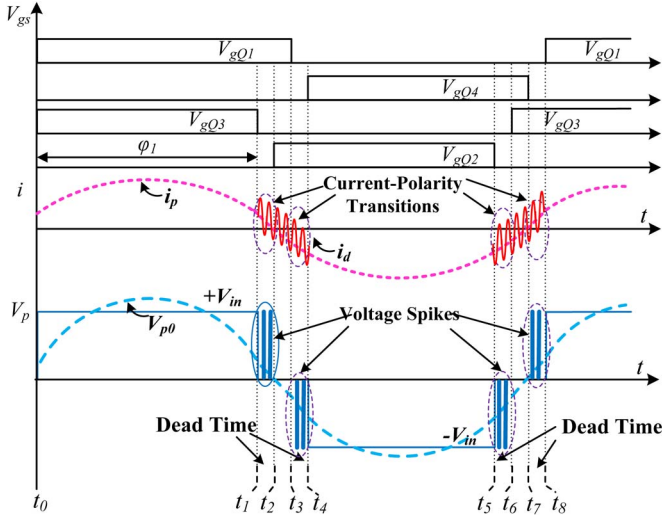


Fig. 6. Conditions of data-carrier influence to power inverter.

The occurrence condition and the waveforms of the spikes are shown in Fig. 6. In Stage 1  $[t_1, t_2]$ ,  $Q_1$  is open and  $Q_{2-4}$  are closed. The current path of the  $L_1C_1$  loop is determined by the polarity of the current  $(i_p + i_d)$ . For  $i_d$  being a high-frequency current, if  $(i_p + i_d)$  is positive, the current flows through MOSFET  $Q_1$  and the diode in  $Q_2$ ; thus, the output voltage  $V_p$  of the inverter is zero. If  $(i_p + i_d)$  becomes negative, the current passes through  $Q_1$  and the diode of  $Q_3$ ; thus, the output  $V_p$  is equal to  $V_{in}$ , which leads to spikes of inverter output in the dead-time period.

In Stage 2  $[t_2, t_3]$ ,  $Q_1$  and  $Q_2$  are turned on. Although the polarity of  $(i_p + i_d)$  changes, the current path is fixed to  $Q_1$  and  $Q_2$ , which will not cause output spikes in the primary inverter.

From the aforementioned analysis, it is concluded that the spikes may occur at the period of dead time. Assuming  $i_p$  and  $i_d$  are sinusoidal

$$i_p(t) = I_p \sin(\omega_p t + \theta_p) \quad (3)$$

$$i_d(t) = I_d \sin(\omega_d t + \theta_d) \quad (4)$$

where  $I_p$  and  $I_d$  are the amplitude of the power carrier and data carrier, respectively.

Assuming the current amplitude of the power carrier is much greater than the data carrier, the sufficient condition, which can avoid the spike influenced by data carrier, is the slow rate of the power carrier at zero crossing point should be greater than the slow rate of the data carrier at any time, which can be expressed as

$$\left. \frac{di_p(t)}{dt} \right|_{(\omega_p t + \theta_p = 0)} > \frac{di_d(t)}{dt}. \quad (5)$$

The aforementioned equation can be simplified as

$$\frac{I_p}{I_d} > \frac{\omega_d}{\omega_p} \quad (6)$$

or

$$V_{L1p} > V_{L1d} \quad (7)$$

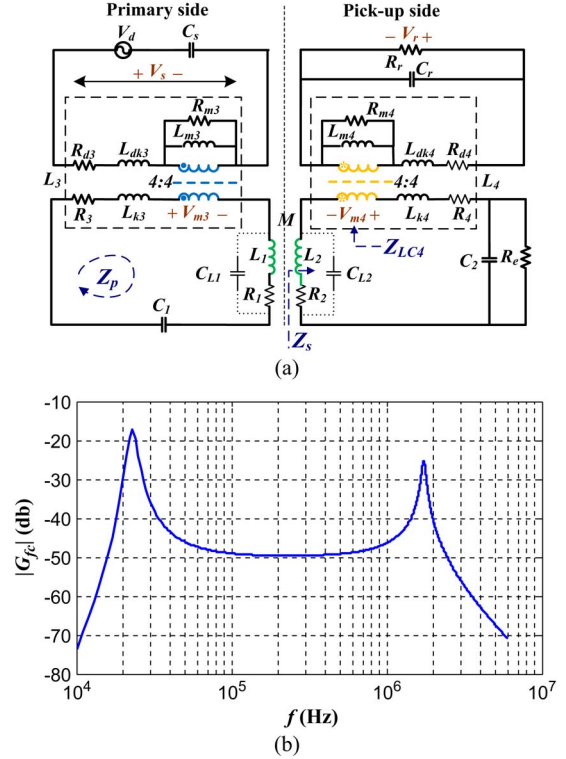


Fig. 7. Circuit model and bode plot of the forward channel. (a) Circuit model of the forward channel. (b) Bode plot of the forward channel ( $M = 23 \mu\text{H}$ ).

where  $V_{L1p}$  and  $V_{L1d}$  are the voltage drops on inductor  $L_1$  by power carrier and data carrier, respectively.

Equation (7) can be easily satisfied in the proposed system during data transmission since the initial voltage for communication is far less than power transfer. On the pickup side, the high-frequency current of data carrier is absorbed by the parallel capacitor  $C_2$ ; thus, it will not reach to the load and interfere with the power output.

#### IV. COMMUNICATION CHANNEL MODELING

In the proposed system, the bidirectional communication is achieved by the magnetic induction communication techniques [29]. The communication antenna is the same coreless coil for power delivery. Compared with the wireless RF communication, the interaction between two sides is mainly nonradiated magnetic field couplings, and the communication channel is represented as a circuit model.

##### A. Forward Communication Channel

The circuit model of forward communication channel is given in Fig. 7(a). Data signal is transmitted from  $V_d$  and received in  $V_r$  at the other side. In the transmitter side, the capacitor  $C_s$  resonates with the primary side of coupled inductor to amplify output power. In the receiver side, the resonant frequency of the capacitor  $C_r$  and coupled inductor is tuned to the data-carrier angular frequency  $\omega_d$ , and the receiver network works as a narrow bandpass filter to diminish the interference from the power carrier.

The coupled inductors can also be considered as signal transformers, whose equivalent circuits are shown in Fig. 7(a), where  $L_{k3}$ ,  $L_{dk3}$  and  $L_{k4}$ ,  $L_{dk4}$  are the leakage inductances,  $L_{m3}$  and  $L_{m4}$  are the magnetizing inductances,  $R_3$ ,  $R_{d3}$  and  $R_4$ ,  $R_{d4}$  are the winding resistances, and  $R_{m3}$  and  $R_{m4}$  are the core loss resistances of the coupled inductor  $L_3$  and  $L_4$ , respectively.

The angular frequency of the data carrier is given by

$$\omega_d = 2\pi f_d = \frac{1}{\sqrt{(L_{dk3} + L_{m3})C_s}} = \frac{1}{\sqrt{(L_{dk4} + L_{m4})C_r}}. \quad (8)$$

The data-carrier frequency  $f_d$  is set at 1.67 MHz for data communication; thus, the skin and proximity effects need to be taken into consideration in this frequency range. The parasitic capacitance of the power coil is depicted as  $C_{L1}$  and  $C_{L2}$ ; and the parasitic resistance  $R_{1-4}$ ,  $R_{d3}$ , and  $R_{d4}$  are taken into consideration in the megahertz frequency range. The parasitic capacitance of the coupled inductor can be neglected because they are small enough even at the data-carrier frequency.

From Fig. 7(a), the equivalent impedance of the signal receiver network in the forward channel is

$$Z_{LC4}(\omega) = \frac{1}{\frac{1}{j\omega L_{m4}} + \frac{1}{R_{m4}} + \frac{1}{j\omega L_{dk4} + R_{d4} + 1/(\omega C_r + 1/R_r)}}. \quad (9)$$

The pickup impedance  $Z_s(\omega)$  is expressed as

$$Z_s(\omega) = j\omega L_2 + R_2 + \frac{1}{j\omega C_2 + 1/R_e} + Z_{LC4}(\omega) + R_4 + j\omega L_{k4} \quad (10)$$

where  $R_e$  is the equivalence of the rectifier load.

The reflected impedance  $Z_{rs}(\omega)$  to the primary side is indicated by

$$Z_{rs}(\omega) = \frac{\omega^2 M^2}{Z_s(\omega)}. \quad (11)$$

Ignoring the impedance of the signal coupled inductor, which is relatively small compared with the impedance of  $L_1$ , the primary loop impedance is described as

$$Z_p(\omega) = j\omega L_1 + R_1 + \frac{1}{j\omega C_1} + Z_{rs}(\omega). \quad (12)$$

The transfer function of the coupled inductor  $L_4$  is

$$G_{L4}(\omega) = \frac{V_r}{V_{m4}} = \frac{1/(j\omega C_r + 1/R_r)}{j\omega L_{dk4} + R_{d4} + 1/(j\omega C_r + 1/R_r)}. \quad (13)$$

For the impedance of the coupled inductor is far lower than the impedance of the power inductor coil, the transfer function of the coupled inductor  $L_3$  is

$$G_{L3}(\omega) = \frac{V_{m3}}{V_s} = \frac{1/(1/j\omega L_{m3} + 1/R_{m3}))}{(j\omega L_{dk3} + R_{d3} + 1/(1/j\omega L_{m3} + 1/R_{m3}))}. \quad (14)$$

From (9)–(14), the transfer function of forward channel from the pickup side of signal transmitter coupled inductor  $G_{fc}(\omega)$  is

$$G_{fc}(\omega) = \frac{V_r}{V_s} = \frac{j\omega M}{Z_p(\omega)} \frac{Z_{LC4}(\omega)}{Z_s(\omega)} G_{L4}(\omega) G_{L3}(\omega). \quad (15)$$

With parameters listed in Table I, the bode plot of  $G_{fc}(\omega)$  is shown in Fig. 7(b). It is clear that two poles exist in the system, one is the power transfer frequency and the other is data-carrier frequency.

Define  $Q_S$  as transmitter quality factor

$$Q_S = \frac{V_s(\omega_d)}{V_d(\omega_d)}. \quad (16)$$

For the proposed system, the value of the  $Q_S$  is determined according to the requirement of data-carrier amplitude by selecting proper capacitance.

The transfer gain at the data-carrier angular frequency  $\omega_d$  can be simplified as follows:

$$Z_s(\omega_d) \approx j\omega_d L_2 + Z_{LC4}(\omega_d). \quad (17)$$

Define the signal receiver quality factor as  $Q_R = (Z_{LC4}(\omega_d)/\omega_d L_{m4})$ ; thus,

$$Z_{rs}(\omega_d) = \frac{\omega_d^2 M^2}{Z_s(\omega_d)} \approx -\frac{j\omega_d M^2}{L_2 - jQ_R L_{m4}} \quad (18)$$

$$Z_p(\omega_d) \approx j\omega_d L_1 - \frac{j\omega_d M^2}{L_2 - jQ_R L_{m4}}. \quad (19)$$

Suppose  $L_{dk3-4}$  are far less than  $L_{m3-4}$ , and  $G_{L3}(\omega_d) \approx G_{L4}(\omega_d) \approx 1$ , the gain of the forward communication channel is simplified

$$\begin{aligned} |G_{fc}(\omega_d)| &= \left| \frac{V_r}{V_s} \right| \approx \left| \frac{j\omega_d M}{Z_p(\omega_d)} \frac{Z_{LC4}(\omega_d)}{Z_s(\omega_d)} \right| \\ &= \left| \frac{Q_R L_{m4} L_2 M}{L_1 L_2 (L_2 - jQ_R L_{m4}) - M^2} \right|. \end{aligned} \quad (20)$$

From (20), two conclusions are obtained: the quality factor of the signal coupled inductor  $Q_R$  is important for the gain of signal transmission; the mutual inductance of the power coupled coils has great influence for the signal transfer gain, and it can be online calculated according to the amplitude demodulated by the receiver circuit if all other parameters are determined.

## B. Backward Communication Channel

As depicted in Fig. 8(a), the backward communication channel has similar characteristics as the forward communication channel, and the equivalent impedances are

$$Z_{LC3R}(\omega) = \frac{1}{\frac{1}{j\omega L_{m3}} + \frac{1}{R_{m3}} + \frac{1}{j\omega L_{dk3} + R_{d3} + 1/(\omega C_r + 1/R_r)}} \quad (21)$$

$$Z_{pR}(\omega) = j\omega L_1 + R_1 + 1/j\omega C_1 + Z_{LC3}(\omega) + R_3 + j\omega L_{k3} \quad (22)$$

$$Z_{rsR}(\omega) = \frac{\omega^2 M^2}{Z_{pR}(\omega)} \quad (23)$$

$$Z_{sR}(\omega) = j\omega L_2 + R_2 + \frac{1}{j\omega C_2 + 1/R_e} + Z_{rsR}(\omega). \quad (24)$$

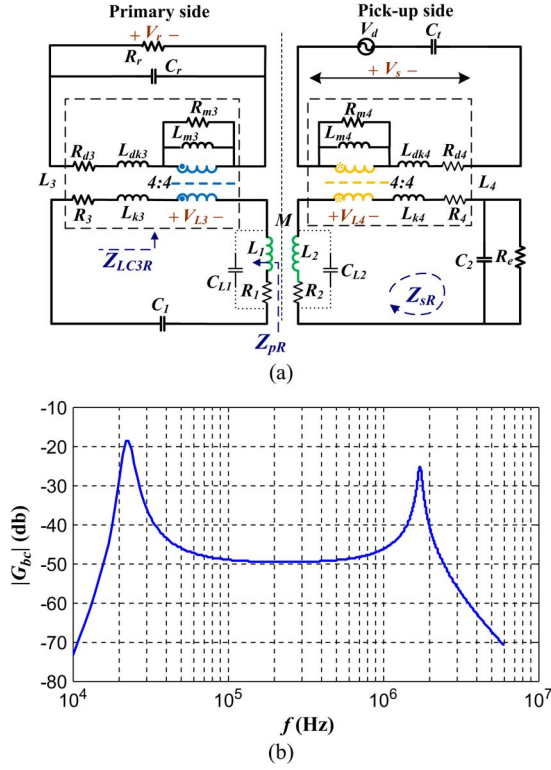


Fig. 8. Circuit model and bode plot of the backward channel. (a) Circuit model of the backward channel. (b) Bode plot of the backward channel ( $M = 23 \mu\text{H}$ ).

The transfer function of the coupled inductor  $L_3$  is

$$G_{L3R}(\omega) = \frac{V_r}{V_{L3}} = \frac{1/(j\omega C_r + 1/R_r)}{(j\omega L_{dk3} + R_{d3} + 1/(j\omega C_r + 1/R_r))}. \quad (25)$$

The transfer function of the coupled inductor  $L_4$  is

$$G_{L4R}(\omega) = \frac{V_{L4}}{V_s} = \frac{1/(1/j\omega L_{m4} + 1/R_{m4}))}{(j\omega L_{dk4} + R_{d4} + 1/(1/j\omega L_{m4} + 1/R_{m4}))}. \quad (26)$$

The transfer function of backward channel from the pickup side of signal transmitter coupled inductor is

$$G_{bc}(\omega) = \frac{V_r}{V_s} = \frac{j\omega M}{Z_{pR}(\omega)} \frac{Z_{LC3R}(\omega)}{Z_{sR}(\omega)} G_{L4R}(\omega) G_{L3R}(\omega). \quad (27)$$

The bode plot of the transfer function  $G_{bc}(\omega)$  is shown in Fig. 8(b), which shows that the system has two poles.

A conventional WPT system is a narrow-band system, which usually has only one pole, the power resonant pole. For the proposed WPT system, the transfer functions of both the forward and backward communication channels contain two poles. The one at 22.4 kHz is induced by the power resonant pole and brings about noises to communication channel, and the other one near 1.67 MHz is created for data transmission by the  $LC$  network. The available band of the proposed system is expanded by adding a high-frequency pole for data transmission, which enables the system to transfer power and data via the same inductive link.

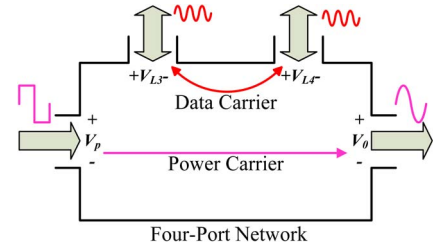


Fig. 9. Four-port network of the wireless power and data transmission system.

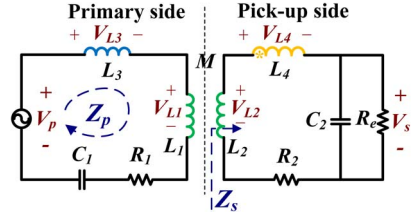


Fig. 10. Equivalent circuit of crosstalk interference.

## V. CROSSTALK ANALYSIS

The crosstalk interference from the power transmission to the reliability of the bidirectional communication is analyzed here.

As shown in Fig. 9, the proposed system can be represented as a four-port network. The power is transferred from the power port “ $V_p$ ” to “ $V_o$ ,” and the data is exchanged between the data ports: “ $V_{L3}$ ” and “ $V_{L4}$ .” The power carrier and the data carrier, reach to each port with different transfer functions. From the analysis in Section II, the power ports are approximately short circuited at the data-carrier frequency  $\omega_d$ ; thus, the data carrier has small interference from power delivery. Nevertheless, the power carrier is a large noise for data communication; thus, it is important to predict the value of the crosstalk from the power transfer.

As discussed in Section III, the equivalent impedance of the communication cells can be simplified as  $L_3$  and  $L_4$  at the power-carrier frequency  $\omega_p$ , which means no difference between the equivalent circuit for the forward channel and backward channel.

The equivalent circuit model of the crosstalk is given in Fig. 10, and the parasitic capacitance of the coils and the leakage inductance of the coupled inductors are neglected since it will not influence the following analysis.

The noise transfer function  $G_{N3}(\omega)$  and  $G_{N4}(\omega)$  are

$$G_{N3}(\omega_p) = \frac{V_{L3}(\omega_p)}{V_p} = \frac{j\omega_p L_3}{Z_p(\omega_p)} \quad (28)$$

$$G_{N4}(\omega_p) = \frac{V_{L4}(\omega_p)}{V_p} = \frac{j\omega_p M}{Z_s(\omega_p)} \frac{j\omega_p L_4}{Z_p(\omega_p)} \quad (29)$$

where  $Z_p(\omega)$  and  $Z_s(\omega)$  are presented in (9)–(11).

Letting  $L_1 + L_3 = L'_1$ ,  $L_2 + L_4 = L'_2$  and according to (2), the aforementioned equations can be calculated by

$$Z_s(\omega_p) = R_2 + j\omega_p L'_2 + \frac{1}{j\omega_p C_2 + 1/R_e} = R_2 + \frac{j\omega_p L'_2}{j\omega_p R_e C_2 + 1} \quad (30)$$

$$Z_{rs}(\omega_p) = \frac{\omega_p^2 M^2}{Z_s(\omega_p)} = \frac{\omega_p^2 M^2 R_e C_2}{L_2'} - \frac{\omega_p M^2}{L_2'} j \quad (31)$$

$$Z_p(\omega_p) = R_1 + \frac{\omega_p^2 M^2 R_e C_2}{L_2'} - \frac{\omega_p M^2}{L_2'} j. \quad (32)$$

From Fig. 8(a), the voltage of the primary power coil is

$$V_{L1}(\omega_p) = \frac{j\omega_p L_1 + Z_{rs}(\omega_p)}{Z_p(\omega_p)} V_p(\omega_p). \quad (33)$$

If the coupling coefficient of the power coil is small and  $Z_{rs}(\omega_p)$  is ignored, from (28) and (33), it can be concluded that

$$\frac{V_{L3}(\omega_p)}{V_{L1}(\omega_p)} \approx \frac{L_3}{L_1'}. \quad (34)$$

Similarly, the voltage of the pickup side power coil is

$$V_{L2}(\omega_p) = \frac{j\omega_p M}{Z_s(\omega_p)} \frac{1/(1/R_e + j\omega_p C_2)}{Z_p(\omega_p)} V_p(\omega_p). \quad (35)$$

For  $R_e \gg 1/(\omega_p C_2)$ , it can be inferred

$$\frac{V_{L4}(\omega_p)}{V_{L2}(\omega_p)} \approx \frac{L_4}{L_2'}. \quad (36)$$

Equations (34) and (36) can be used to estimate the crosstalk interference in a power condition, and it can be concluded that the smaller the signal coupling inductance is, the lower the crosstalk interference should be. However, for a WPT system where the inductance of the coupled coil and signal coupling inductor are predetermined, the SNR can be only increased by magnifying the output of data carrier. In addition, increasing the output of data carrier will increase the power consumed by the data communication, which will add more power losses to the system.

## VI. COMMUNICATION CIRCUIT DESIGN

In the proposed scheme, half-duplex communication between the primary side and the pickup side is implemented, with the transmitter and receiver circuits are merged into the communication cells shown in Fig. 11(a).

The status of the communication cells are controlled by  $Q_{5-8}$ . In receiver mode,  $Q_{5-6}$  are turned off and  $Q_{7-8}$  are turned on. In transmitter mode,  $Q_{7-8}$  are turned off, and on-off-keying modulation is employed to transmit data. If the transmitter sends bit "1",  $Q_5$  and  $Q_6$  work as complementary switch at the frequency  $f_c$  for a bit-period  $T_b$ ; If the transmitter sends bit "0",  $Q_5$  and  $Q_6$  are turned off for a bit-period  $T_b$ . The communication rate of the system is determined by  $T_b$ , and the drive signal and output waveform of the communication cell is present in Fig. 11(b).

As the transmitter sends carrier signal,  $Q_5$  and  $Q_6$  work as complementary, and the switching duty cycle is set at 0.5 with the frequency of data carrier. The output power of the half bridge can be well-designed by selecting proper capacitance  $C_t$ .

When the communication cell operates in receiver mode, carrier signal from the other side is received in  $V_R$  and processed by the demodulation circuits, which is illustrated in Fig. 12. The

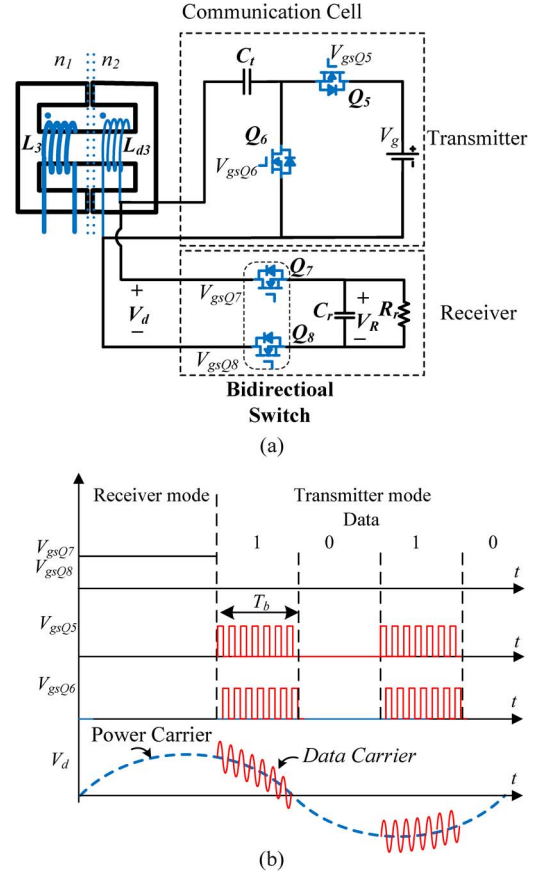


Fig. 11. Circuit and drive signal of the communication cell. (a) Schematic of the communication cell. (b) Drive signal and waveforms of the communication cell.

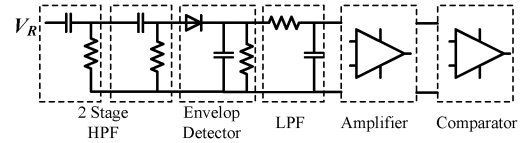


Fig. 12. Schematic circuit of demodulation module.

data carrier is sent into a two-stage high-pass filter (HPF) at first to eliminate the power carrier, whose cutoff frequency is set at about 1 MHz.

The output of the HPF is processed by an amplitude detector circuits, which consist of an envelope detector, a low-pass filter (LPF), an amplifier and a comparator. The envelop detector, which contains a diode, a capacitor and a resistor, is widely used in signal demodulation for its low costs and easy implementation. The  $RC$  LPF is responsible for further diminishing high-frequency noise. To reach a reference voltage, the amplifier is used to amplify the data amplitude. The last part of the demodulation unit is the comparator, and the decoded data is sent to the MCU with reference voltages, which is compatible with traditional series communication interface.

## VII. EXPERIMENT VERIFICATION

A 500-W prototype has been built up to verify the proposed method, with the parameters listed in Table II. The schematic circuit is the same as Fig. 3, and the input voltage is 40 V. The



TABLE II  
PARAMETERS OF THE 500-W PROTOTYPE

Components	Parameters
$P_{out}$ (Output power)	500 W
$P_{data}$ (Power of data transmitting)	2 W
$V_{in}$ (Input DC voltage of power transfer)	40 V
$V_d$ (Input DC voltage of data transfer)	10 V
$V_o$ (Output DC voltage)	200 V
$f_p$ (Power carrier frequency)	22.4 kHz
$f_d$ (Data-carrier frequency)	1.67 MHz
$\eta$ (Power transfer efficiency)	86%
$d$ (Air gap)	7.5 cm
$r_1$ and $r_2$ (Winding radius)	7.5 cm
SNR of data carrier ( $20\log[V_{L4}(\omega_d)/V_{L4}(\omega_p)]$ )	-16 dB
Power switch $Q_{1-4}$	IRFP4227
Signal switch $Q_{5-8}$	SI2327

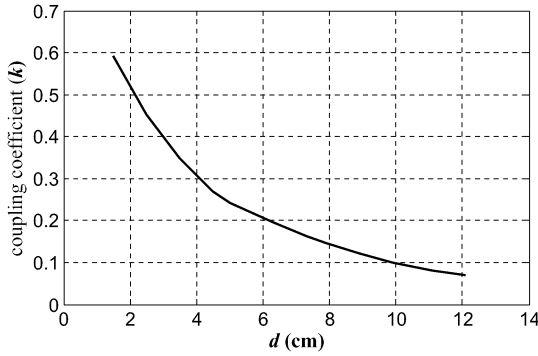


Fig. 13. Relationship between coupling coefficient and distance.

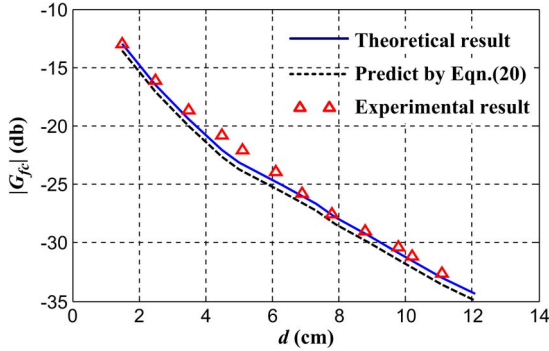


Fig. 14. Relationship between the gain of forward channel and distance.

multiple-layer coils are wound on circular frames without any ferrite core. The primary side and the pickup side are controlled independently by TMS320F28035 MCUs to regulate power and data transmission.

The mutual inductance  $M$  between primary and pickup sides for any position and sizes can be estimated by formula [7], but the result usually is not accurate. In this experiment, the mutual inductance of the coils is calculated according to the inductance of the coupled coils in series-aiding connection and in series-opposing connection, which is measured by LCR meter. The relationship between the coupling coefficient  $k$  and the distance of the two coils is depicted in Fig. 13.

The gain of the forward channel at 1.67 MHz versus the air gap distance is shown in Fig. 14, and the experimental results are compared with the theoretical result calculated by MATLAB, where the solid line is calculated from (15) when  $\omega = \omega_d$

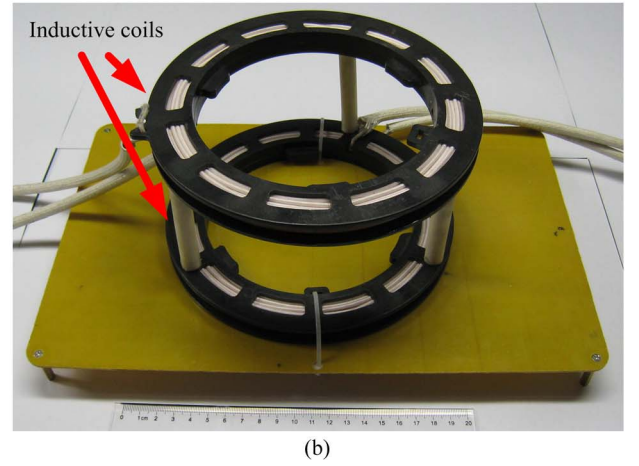
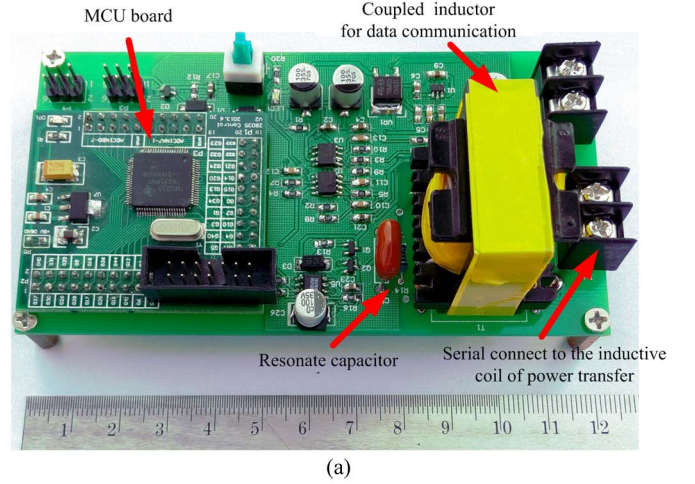


Fig. 15. Picture of the communication board and inductive coils. (a) Communication board. (b) Inductive coils.

and the dashed line are calculated using the simplified (20). Experimental results and the theoretical calculation are in good agreement, which verifies the modeling of the communication channel in Section IV.

The printed circuit board of the communication cell and the inductive coils for power and data transfer are depicted in Fig. 15. The waveforms in the power coupled coils are shown in Fig. 16, from which the data carrier can be only seen in the pickup side coil, whereas backward communication, for the ratio of amplitude between data carrier and power carrier is relatively big.

Fig. 17(a) shows the waveforms of forward communication at the data rate of 20 kb/s. The transmission distance is set 7.5 cm and the coils mutual coefficient is about 0.15.  $V_{din}$  is the bit stream sent by transmitter, and  $V_{L3}$  is the waveform in the signal coupling inductor at pickup side, and  $V_{L4}$  is the waveform in the signal coupling inductor at primary side, and  $V_{dout}$  is the bit stream received.

The amplitudes of frequency  $\omega_p$  and  $\omega_d$  components are listed in Table III, which is calculated by fast Fourier Transform according to the sampled data. It can be seen that

$$\begin{aligned} V_{L3}(\omega_p)/V_{L1}(\omega_p) &= 0.024 \approx L_3/L'_1 = 0.025 \\ V_{L4}(\omega_p)/V_{L2}(\omega_p) &= 0.027 \approx L_4/L'_2 = 0.025. \end{aligned} \quad (37)$$



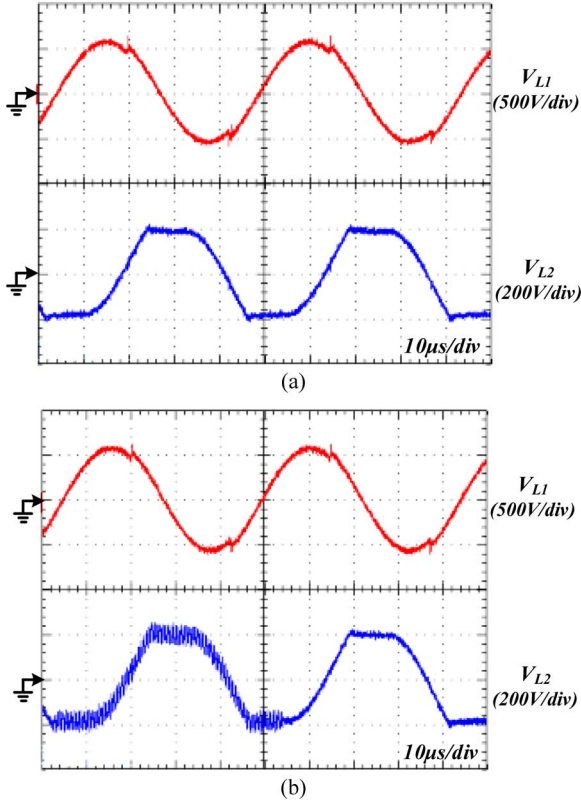


Fig. 16. Waveforms of the primary and pickup side in power inductive coils. (a) Forward communication. (b) Backward communication.

The experimental crosstalk noises are close to predicted results in (34) and (36). The data-carrier transmission gain in forward channel is  $20 \log(V_{L3}(\omega_d)/V_{L4}(\omega_d)) = -28$  dB, which is consistent with the analysis in communication channel modeling.

Fig. 17(b) shows the waveforms of backward communication at the data rate of 20 kb/s, which is similar with the waveforms of forward communication.

To compare the efficiency of the proposed system with conventional WPT system, the coupled inductor in the communication board is short circuited and the power transfer efficiency is measured. It shows that the power transfer efficiency of the proposed system is almost the same as conventional WPT system (the power of signal transfer is ignored). The reason is that the inductance of the data signal coupling inductor is small and the loss of the inductor is very low. However, the communication circuits, including modulation and demodulation circuits, need extra power source, which also bring about additional power loss. In this experiment, it achieves  $-16$  dB of SNR and consumes only 2 W of additional power (0.4% of 500-W power transfer), which is quite small comparing with the power transferred.

However, if applying this method to a low power system, the efficiency of power transfer would be reduced significantly. On the other side, if employing this method to WPT applications operating in several megahertz range, the data carrier should operate in several 10 megahertz to avoid crosstalk interference, and additional circuits are needed to deal with the

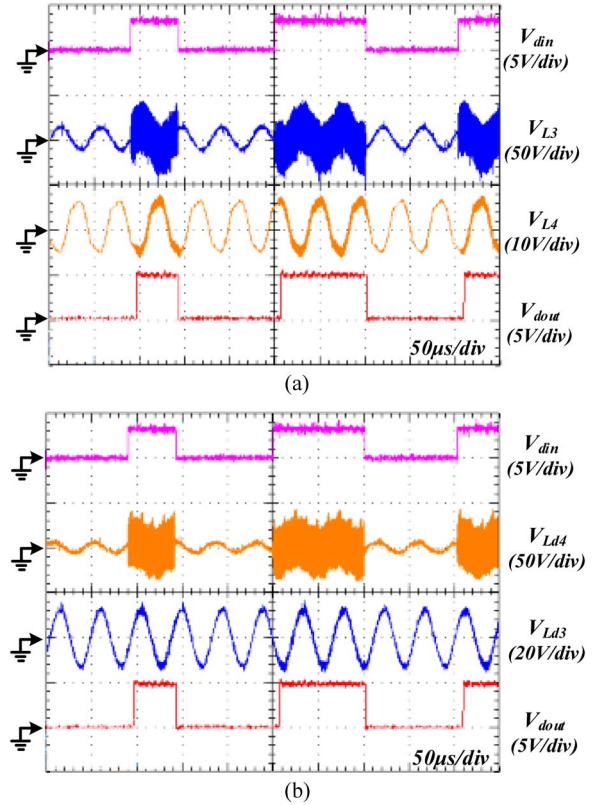


Fig. 17. Waveforms of forward and backward communication. (a) Forward communication. (b) Backward communication.

TABLE III  
VOLTAGE AMPLITUDE OF FREQUENCY  $\omega_p$  AND  $\omega_d$  COMPONENTS IN INDUCTOR  $L_{1\sim4}$  WHILE FORWARD COMMUNICATION

	Frequency $\omega_p$	Frequency $\omega_d$
$V_{L1}$	580V	22.6V
$V_{L2}$	218V	1.0V
$V_{L3}$	14.0V	24.8V
$V_{L4}$	5.9V	0.95V

high-frequency carrier, which increase the volume of the system. So, in low-power WPT applications, this method has no advantage to conventional FSK/LSK method.

## VIII. CONCLUSION

For WPT systems, communication between the primary side and the pickup side is important. This paper proposed a novel method that integrates near-field communication with high-power WPT. In this system, the power carrier and data carrier employ the same coil to transmit power and data by means of frequency division duplexing.

The performance of the power and data transfer, as well as the cross-effect between power transfer and data communication, are analyzed in detail. It has been shown that the power and data can share a pair of common coupled coils and be controlled independently. The results obtained from a 500-W experimental platform are in line with the theoretical analysis, which verify the effectiveness of the proposed method.

The communication channel between two sides, which has acquired 20 kb/s data rate in this paper, can be used for close-loop control. In the pickup side, the output voltage and current are sampled and sent back to the primary side, and then, the controller in the primary side changes its frequency to regulate the output voltage or current in pickup side. For WPT system with about 20-kHz power carrier, the 20-kb/s data rate is fast enough for the control loop, and it can be promoted by increasing the carrier frequency and improving the modulation/demodulation method. Another potential application of this method is that the bit stream of communication can be employed as a synchronous clock for bidirectional WPT. On the other side, the mutual inductance of the coils can be calculated by measuring the amplitude of the received data carrier, which can be utilized to improve power control strategy.

The proposed method aims for the applications of high-power WPT with low frequency. However, due to the power losses in communication resonant tank, the total efficiency of the WPT system decreases slightly, so that this method is not suitable for the communication in low-power WPT system with high-frequency carrier, which is dominated by FSK/LSK method.

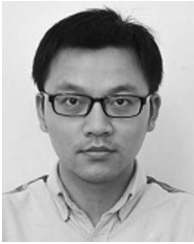
## REFERENCES

- [1] J. C. Schuder and H. E. Stephenson, "Energy transport to a coil which circumscribes a ferrite core and is implanted within the body," *IEEE Trans. Bio-Med. Eng.*, vol. BME-12, no. 3/4, pp. 154–163, Jul.–Oct. 1965.
- [2] D. Ahn and S. Hong, "Wireless power transmission with self-regulated output voltage for biomedical implant," *IEEE Trans. Ind. Electron.*, vol. 61, no. 5, pp. 2225–2235, May 2014.
- [3] S. Y. R. Hui and W. W. C. Ho, "A new generation of universal contactless battery charging platform for portable consumer electronic equipment," *IEEE Trans. Power Electron.*, vol. 20, no. 3, pp. 620–627, May 2005.
- [4] S. Y. R. Hui, "Planar wireless charging technology for portable electronic products and Qi," *Proc. IEEE*, vol. 101, no. 6, pp. 1290–1301, Jun. 2013.
- [5] R. Tseng, B. von Novak, S. Shevde, and K. A. Grajski, "Introduction to the alliance for wireless power loosely-coupled wireless power transfer system specification version 1.0," in *Proc. IEEE Wireless Power Transfer Conf.*, Perugia, Italy, May 2013, pp. 79–83.
- [6] M. Yilmaz and P. T. Krein, "Review of battery charger topologies, charging power levels, and infrastructure for plug-in electric and hybrid vehicles," *IEEE Trans. Power Electron.*, vol. 28, no. 5, pp. 2151–2169, May 2013.
- [7] J. Sallan, J. L. Villa, A. Llombart, and J. F. Sanz, "Optimal design of ICPT systems applied to electric vehicle battery charge," *IEEE Trans. Ind. Electron.*, vol. 56, no. 6, pp. 2140–2149, Jun. 2009.
- [8] M. Budhia, J. T. Boys, G. A. Covic, and C. Huang, "Development of a single-sided flux magnetic coupler for electric vehicle IPT charging systems," *IEEE Trans. Power Electron.*, vol. 60, no. 1, pp. 318–328, Jan. 2013.
- [9] J. Shin *et al.*, "Design and implementation of shaped magnetic-resonance-based wireless power transfer system for roadway-powered moving electric vehicles," *IEEE Trans. Ind. Electron.*, vol. 61, no. 3, pp. 1179–1192, Mar. 2014.
- [10] S. Chopra and P. Bauer, "Driving range extension of EV with on-road contactless power transfer: A case study," *IEEE Trans. Ind. Electron.*, vol. 60, no. 1, pp. 329–338, Jan. 2013.
- [11] U. K. Madawala and D. J. Thrimawithana, "A bidirectional inductive power interface for electric vehicles in V2G systems," *IEEE Trans. Ind. Electron.*, vol. 58, no. 10, pp. 4789–4796, Oct. 2011.
- [12] S. Ping, A. P. Hu, S. Malpas, and D. Budgett, "A frequency control method for regulating wireless power to implantable devices," *IEEE Trans. Biomed. Circuits Syst.*, vol. 2, no. 1, pp. 22–29, Mar. 2008.
- [13] V. J. Brusamarello, Y. B. Blauth, R. de Azambuja, I. Muller, and F. R. de Sousa, "Power transfer with an inductive link and wireless tuning," *IEEE Trans. Instrum. Meas.*, vol. 62, no. 5, pp. 924–931, May 2013.
- [14] Z. Wang, Y. Li, Y. Sun, C. Tang, and X. Lv, "Load detection model of voltage-fed inductive power transfer system," *IEEE Trans. Power Electron.*, vol. 28, no. 11, pp. 5233–5243, Nov. 2013.
- [15] R. Johari, J. V. Krogmeier, and D. J. Love, "Analysis and practical considerations in implementing multiple transmitters for wireless power transfer via coupled magnetic resonance," *IEEE Trans. Ind. Electron.*, vol. 61, no. 4, pp. 1774–1783, Apr. 2014.
- [16] X. Ju, L. Dong, X. Huang, and X. Liao, "Switching technique for inductive power transfer at high-Q regimes," *IEEE Trans. Ind. Electron.*, vol. 62, no. 4, pp. 2164–2173, Apr. 2015.
- [17] D. J. Thrimawithana, U. K. Madawala, and M. Neath, "A synchronization technique for bidirectional IPT systems," *IEEE Trans. Ind. Electron.*, vol. 60, no. 1, pp. 301–309, Jan. 2013.
- [18] G. Yilmaz, O. Atasoy, and C. Dehollain, "Wireless energy and data transfer for in-vivo epileptic focus localization," *IEEE Sens. J.*, vol. 13, no. 11, pp. 4172–4179, Nov. 2013.
- [19] G. Wang, P. Wang, Y. Tang, and W. Liu, "Analysis of dual band power and data telemetry for biomedical implants," *IEEE Trans. Biomed. Circuits Syst.*, vol. 6, no. 3, pp. 208–215, Jun. 2012.
- [20] G. Simard, M. Sawan, and D. Massicotte, "High-speed OQPSK and efficient power transfer through inductive link for biomedical implants," *IEEE Trans. Biomed. Circuits Syst.*, vol. 4, no. 3, pp. 192–200, Jun. 2010.
- [21] C. Yu, R. Lu, C. Su, and C. Zhu, "Study on wireless energy and data transmission for long-range projectile," *IEEE Trans. Plasma Sci.*, vol. 41, no. 5, pp. 1370–1375, May 2013.
- [22] U. K. Madawala, J. Stichbury, and S. Walker, "Contactless power transfer with two-way communication," in *Proc. IEEE Conf. Ind. Electron.*, Busan, Korea, Nov. 2004, pp. 3071–3075.
- [23] W. P. Choi, W. C. Ho, X. Liu, and S. Y. R. Hui, "Bidirectional communication techniques for wireless battery charging systems & portable consumer electronics," in *Proc. IEEE Conf. Appl. Power Electron.*, Palm Springs, CA, USA, 2010, pp. 2251–2257.
- [24] T. Bieler, M. Perrottet, V. Nguyen, and Y. Perriard, "Contactless power and information transmission," *IEEE Trans. Ind. Appl.*, vol. 38, no. 5, pp. 1266–1272, Sep./Oct., 2002.
- [25] J. Hirai, K. Tae-Woong, and A. Kawamura, "Study on intelligent battery charging using inductive transmission of power and information," *IEEE Trans. Power Electron.*, vol. 15, no. 2, pp. 335–345, Mar. 2000.
- [26] J. Hirai, K. Tae-Woong, and A. Kawamura, "Integral motor with driver and wireless transmission of power and information for autonomous sub-spindle drive," *IEEE Trans. Power Electron.*, vol. 15, no. 1, pp. 13–20, Jan. 2000.
- [27] J. Hirai, K. Tae-Woong, and A. Kawamura, "Study on crosstalk in inductive transmission of power and information," *IEEE Trans. Ind. Electron.*, vol. 46, no. 6, pp. 1174–1182, Dec. 1999.
- [28] E. L. Van Boheemen, J. T. Boys, and G. A. Covic, "Dual-tuning IPT systems for low bandwidth communications," in *Proc. IEEE Conf. Ind. Electron. Appl.*, Harbin, China, 2007, pp. 586–591.
- [29] Z. Sun and I. F. Akyildiz, "Magnetic induction communications for wireless underground sensor networks," *IEEE Trans. Antennas Propag.*, vol. 58, no. 7, pp. 2426–2435, Jul. 2010.



**Jiande Wu** (M'11) was born in Zhejiang, China, in 1973. He received the B.Sc., M.Sc., and Ph.D. degrees from the College of Electrical Engineering, Zhejiang University, Hangzhou, China, in 1994, 1997, and 2012, respectively.

Since 1997, he has been a Faculty Member with Zhejiang University, where he is currently an Associate Professor. From 2013 to 2014, he was an Academic Visitor with the University of Strathclyde, Glasgow, U.K. His research interests include embedded communication technology applied in power electronics, power electronics control, and photovoltaic generation systems.



**Chongwen Zhao** (S'13) received the B.Sc. degree from the School of Electronic Engineering, Xidian University, Xi'an, China, in 2011, and the M.Sc. degree from the College of Electrical Engineering, Zhejiang University, Hangzhou, China, in 2014. He is currently working toward the Ph.D. degree in electrical engineering at The University of Tennessee, Knoxville, TN, USA.

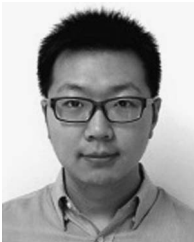
His research interests include wireless power and communication applications and dc-dc power conversion.



**Zhengyu Lin** (S'03–M'05–SM'10) received the B.Sc. and M.Sc. degrees from the College of Electrical Engineering, Zhejiang University, Hangzhou, China, in 1998 and 2001, respectively, and the Ph.D. degree from Heriot-Watt University, Edinburgh, U.K., in 2005.

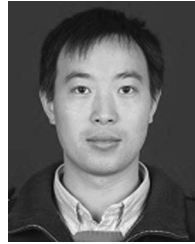
He is currently a Lecturer with Electrical, Electronic, and Power Engineering, Aston University, Birmingham, U.K. He was a Research Associate with The University of Sheffield, Sheffield, U.K., from 2004 to 2006, an R&D

Engineer with Emerson Industrial Automation, Control Techniques PLC, from 2006 to 2011, a Senior Research Scientist with Sharp Laboratories of Europe Ltd. from 2011 to 2012, and a Lecturer with Coventry University from 2013 to 2014. His research interests include power electronics and applications in renewable energy, energy storage, motor drives, and power systems.



**Jin Du** (S'11) received the B.S. degree in electrical engineering from Zhejiang University, Hangzhou, China, in 2011, where he is currently working toward the Ph.D. degree in the College of Electrical Engineering.

His current research interests include power optimization of renewable generation and communication techniques applied in power electronics.



**Yihua Hu** (M'13) received the B.S. degree in electrical motor drives in 2003 and the Ph.D. degree in power electronics and drives in 2011 from China University of Mining and Technology, Jiangsu, China.

Between 2011 and 2013, he was with the College of Electrical Engineering, Zhejiang University, Hangzhou, China, as a Postdoctoral Fellow. Between November 2012 and February 2013, he was an Academic Visiting Scholar with the School of Electrical and Electronic Engineering, Newcastle University, Newcastle upon Tyne, U.K. He is currently a Research Associate with the Department of Electronic and Electrical Engineering, University of Strathclyde, Glasgow, U.K. He has published more than 20 technical papers in leading journals and conference proceedings. His research interests include photovoltaic generation systems, dc-dc/dc-ac converters, and electrical motor drives.



**Xiangning He** (M'95–SM'96–F'10) received the B.Sc. and M.Sc. degrees from Nanjing University of Aeronautics and Astronautics, Nanjing, China, in 1982 and 1985, respectively, and the Ph.D. degree from Zhejiang University, Hangzhou, China, in 1989.

From 1985 to 1986, he was an Assistant Engineer with the 608 Institute of Aeronautical Industrial General Company, Zhuzhou, China. From 1989 to 1991, he was a Lecturer with Zhejiang University. In 1991, he received a Fellowship from the Royal Society of the U.K. and conducted research in the Department of Computing and Electrical Engineering, Heriot-Watt University, Edinburgh, U.K., as a Postdoctoral Research Fellow for two years. In 1994, he joined Zhejiang University as an Associate Professor, where he has been a Full Professor since 1996. He is currently the Vice Dean of the College of Electrical Engineering, Zhejiang University. His research interests include power electronics and their industrial applications.